IEEE Access
Multidisciplinary | Rapid Review | Open Access Journal

Received February 20, 2021, accepted March 8, 2021, date of publication March 10, 2021, date of current version March 19, 2021.

Digital Object Identifier 10.1109/ACCESS.2021.3065376

An AC-DC Interleaved ZCS-PWM Boost Converter With Reduced Auxiliary Switch RMS Current Stress

RAMTIN RASOULINEZHAD, (Graduate Student Member, IEEE), ADEL ALI ABOSNINA, (Student Member, IEEE), JAVAD KHODABAKHSH, (Member, IEEE), AND GERRY MOSCHOPOULOS, (Senior Member, IEEE)
Department of Electrical and Computer Engineering, Western University, London, ON N6A 3K7, Canada
Corresponding author: Ramtin Rasoulinezhad (rrasouli@uwo.ca)

ABSTRACT The paper proposes a novel interleaved AC-DC ZCS-PWM boost converter that requires the use of just a single active auxiliary switch to assist in the turning off the main power circuit switches with ZCS. The auxiliary switch can be turned on and off with ZCS and its auxiliary circuit allows the converter to operate without an increase in the main switch peak current or voltage stress. The auxiliary switch in the converter is active for a much shorter time than in most other ZCS-PWM converter, which allows the converter to operate at higher power levels than other previously proposed interleaved ZCS-PWM converter with a single auxiliary switch. The proposed converter's operation is explained in the paper and its key features and design considerations are discussed. Experimental results that confirm the operation of the proposed converter are presented as well.

INDEX TERMS Switch mode power supplies, ac-dc conversion, soft-switching, ZCS-PWM converter.

I. INTRODUCTION

AC-DC boost converters with input power factor correction (PFC) are widely used in industry as their input current can meet harmonic standards set by regulatory agencies [1]–[6]. Especially popular are AC-DC PFC converters that are made up of at least two interleaved boost converter modules, such as the ones proposed in [7]–[16]. With interleaving, the input current of each module can be made to be discontinuous so that the size of their input inductors are reduced as the net input current has a ripple that is comparable to that of a single boost converter module with a large input inductor. Moreover, there is less current stress on the converter components as they handle a fraction of the overall current and the control is easier as more sophisticated control methods needed for continuous current mode (CCM) operation are avoided.

Soft-switching methods for these converters can either be zero-voltage switching (ZVS) if they are implemented with MOSFETs or zero-current switching (ZCS) if implemented with IGBTs. The focus of the paper is on ZCS methods for IGBT converters [18]–[20], [22]–[25], [27]–[34]. Most of these, use an auxiliary circuit that is activated whenever a main converter switch is about to be turned off, gradually diverting current away from the switch so that it can turn off with ZCS. ZCS is beneficial for IGBTs as it eliminates the current tail that would otherwise exist when turning off. This current tail overlaps with the switch voltage and causes significant turn-off losses.

Previously proposed methods in interleaved boost converters have at least one of the following drawbacks:

a) Each module of an interleaved AC-DC boost converter must have its own auxiliary circuit to help its main switch turn off with ZCS, instead of using just one active auxiliary circuit for both main switches. This adds cost to the overall converter [18], [19], [33], [34].
b) Auxiliary circuit components must be placed in the main part of the converter. With more components in the main path of current, conduction losses are increased, and the auxiliary circuit components need to be implemented with higher current rated components [20], [22]–[32], [36]–[38].
c) The auxiliary circuit injects current into the main switches, which increases peak and RMS current stresses. This is typical of resonant-type auxiliary

The associate editor coordinating the review of this manuscript and approving it for publication was Yuh-Shyan Hwang.

circuits. This creates a need for a higher rated device for the main switch and also increases conduction losses that can offset any gain in efficiency caused by the reduction of switching losses [16], [20], [22], [28].

d) The auxiliary switch does not operate with ZCS, but operates with hard-switching instead [17].

e) Generally, in any ZCS-PWM converter, the auxiliary circuit causes the light-load efficiency of the converter to decrease as it produces more losses than it saves for light loads [18]–[20], [23], [25]–[32]. Any active auxiliary circuits that are used to reduce switching losses are effective when the converter is operating with heavy-loads when there is current in the converter to create losses, but less so when the converter is operating with light-loads as there is little current in the converter, thus few current-related losses. These active auxiliary circuits cannot be disengaged from the converter.

f) Energy pumped into the auxiliary circuit when it is activated, from the main converter circuit, is trapped in the auxiliary circuit where it is dissipated. There is no path for at least some of this energy to be transferred to the output [17], [19], [20], [22], [23], [27], [28].

g) The auxiliary circuit increases the voltage stress of the boost diode by a significant amount 20], [23]–[25], [30]–[32], [36]. This is especially true of resonant-type auxiliary circuits that present a negative voltage at the anode of the boost diode while active, which forces the peak voltage stress of the diode to be greater than the output voltage.

h) For a two-module interleaved ZCS-PWM converter that has just a single active auxiliary circuit to help the main switches turn off with ZCS, the auxiliary switch in the circuit must be turned on and off twice during a switching cycle. The switch therefore operates with double the converter switching frequency as a result. If this switch needs to be on for a significant amount of time, then turning it on twice during a switching cycle increases the RMS current stress of the auxiliary switch and thus the auxiliary circuit losses. If an auxiliary switch is to be implemented with a device that is cheaper and that has better switching characteristics than that used for the main switches, the power rating of the converter must be limited so that the auxiliary switch can handle the power in the auxiliary circuit [17], [20], [22], [23], [27]–[31].

An interleaved ZCS-PWM AC-DC boost converter that consisted of two boost converter modules and just one auxiliary switch was proposed by the authors in [40]. Although it addressed a number of the above-mentioned drawbacks, it did not address all of them. In this article, an improved version of the converter is proposed. The proposed converter has none of the above-mentioned drawbacks and can be operated at higher power levels than other previously proposed interleaved ZCS-PWM converters with a single auxiliary switch because the RMS current of the auxiliary switch is significantly reduced.

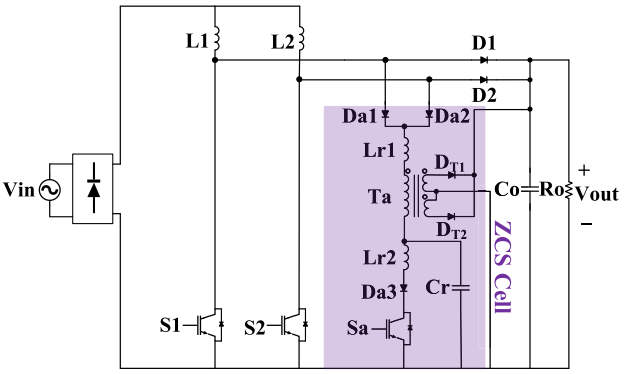

FIGURE 1. Proposed interleaved AC-DC ZCS-PWM boost converter.

In this article, the general principles behind the operation of the proposed converter are discussed and its modes of operation are explained. Guidelines for the design of key auxiliary circuit components are given and the features of the converter are reviewed in detail. The feasibility of the proposed converter is confirmed with results obtained from an experimental prototype.

II. GENERAL CONVERTER PRINCIPLES

The proposed AC-DC converter, shown in Fig. 1, consists of two boost converter modules: one with L_1, S_1 and D_1, the other with L_2, S_2 and D_2. The gating signals of the two main switches, S_1 and S_2 are identical, but shifted 180^o with respect to each other. The currents in L_1 and L_2 are discontinuous and identical, but also shifted 180^o with respect to each other.

The two boost modules are connected to the same auxiliary circuit, which consists of connection diodes D_{a1} and D_{a2}, reverse blocking diode D_{a3}, inductors L_{r1}, L_{r2}, capacitor C_r, and a center tap feed forward transformer T_a which has two diodes D_{T1} and D_{T2}. The auxiliary circuit is activated whenever a main switch is about to be turned off and is active for only a fraction of the switching cycle.

The proposed converter has the following modes of operation for a half switching cycle when duty cycle $D \geq 0.5$ and when S_2 is turned on and S_1 is turned off; Typical waveforms and circuit diagrams for these modes are shown in Fig. 2 and Fig.3 respectively.

The modes of operation for the other half-cycle when S_1 is turned on and S_2 is turned off are identical.

The modes of operation are derived based on the following assumptions:

- Since the AC input voltage can be considered as an DC input source in a very short amount of time, the steady-state analysis is done with DC input voltage.
- The proposed circuit has two boost modules that are designed to be operated in DCM, so the input inductor current of each one will become discontinuous. However, the input current of the converter, which is the sum of the inductor currents, should be continuous.
- The output filter capacitor, C_o, is large enough to be considered as a voltage source V_o.

- All switches, diodes, and passive elements are ideal with no losses.

The description of each mode is presented as follows along with the modal equations that define it. It should be noted that due to page limitations, the only solutions that are shown are those for the equations for Mode 3, as these are related to the ZCS operation of the converter. The solutions to the Mode 3 equations are meant to be an example of the type of solution equations that exist for the converter.

Mode 1 ($t_0 < t < t_1$): This mode begins when switch S_2 is turned on. When switch S_2 is turned on, the rectified voltage is applied to L_2 and leads to a gradual increase of the current through the L_2 and the input current in the input inductor I_{in}. The slope of L_2, which is equal to the slope of S_2, is increased as follows:

$$V_{in} = L_2 \frac{dL_2\,(t_1)}{dt} \tag{1}$$

By integrating from time t_0 to t_1, the main switch current can be written as follows:

$$I_{S2}\,(t_1) = \frac{V_{in}}{L_2}\,(t_1 - t_0) \tag{2}$$

Mode 2 ($t_1 < t < t_2$): This mode begins when the auxiliary switch (S_a) is turned on in preparation to turn off main switch S_1 with ZCS. S_a turns on with ZCS because L_{r2} limits the rise of the switch current. After S_a is turned on, C_r starts to resonate with L_{r2} so that the current in L_{r2} rises while the voltage across C_r decreases. The equations that define this mode are

$$V_{Cr}\,(t_2) = -L_{r2}C_r \frac{d^2}{dt^2} V_{Cr}\,(t_2) \tag{3}$$

$$i_{Lr2}\,(t_2) = i_{Cr}\,(t_2) - C_r \frac{d}{dt^2} V_{Cr}\,(t_2) \tag{4}$$

The initial condition for (3) and (4) are $V_{cr}(0) = V_{cm}$,which is the maximum voltage of the capacitor, and $i_{lr2}(0) = 0$. Solving these equations gives

$$V_{Cr}\,(t_2) = V_{cm} \cos\,(\omega_2 t_2) \tag{5}$$

$$i_{Lr2}\,(t_2) = \frac{V_{cm}}{Z_2} \sin\,(\omega_2 t_2) \tag{6}$$

where $\omega_2 = \frac{1}{\sqrt{L_{r2}C_r}}$ and the characteristic impedance of the auxiliary circuit is defined as $Z_2 = \sqrt{\frac{L_{r2}}{C_r}}$. Mode 2 is finished when the voltage of the auxiliary capacitor V_{cr} reaches to zero. Therefore, the duration of this mode can be calculated by making (5), equal to zero:

$$t_2 - t_1 = \frac{\pi}{2}\sqrt{L_{r2}C_r} \tag{7}$$

The maximum current through the auxiliary circuit can be obtained at the end of this mode by substituting (7) into (6):

$$i_{Lr2}\,(t_2) = \frac{V_{cm}}{Z_2} \sin(\omega_2 \frac{\pi}{2} \frac{1}{\omega_2}) \tag{8}$$

$$i_{Lr2max} = i_{samax} = \frac{V_{cm}}{Z_2} \tag{9}$$

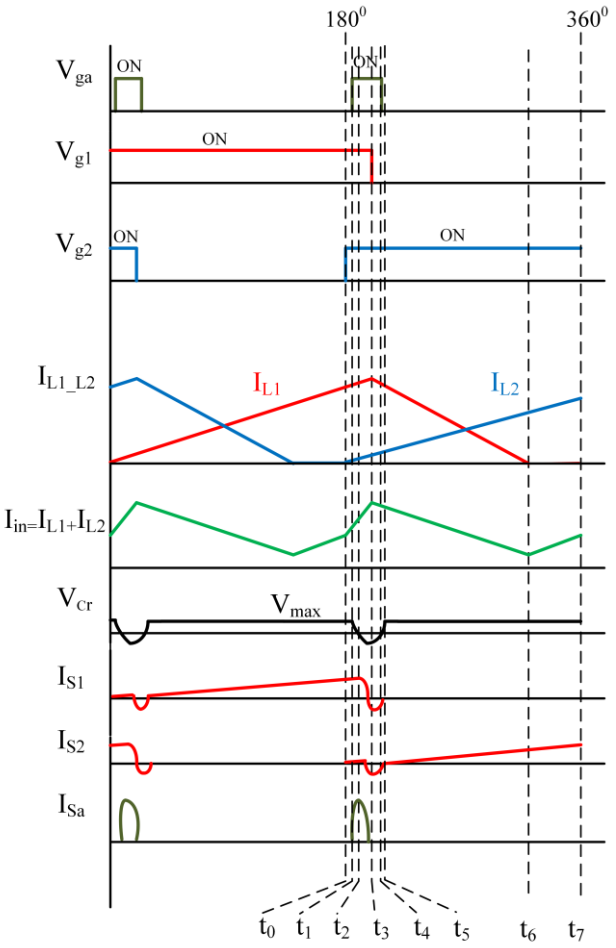

FIGURE 2. Typical waveforms.

Mode 3 ($t_2 < t < t_3$): This mode begins when the voltage across C_r, V_{Cr}, is zero. During this mode, V_{cr} is charged to a negative voltage and D_{a1} and D_{a2} start to conduct. D_{T1} starts to conduct so ccirculating energy from the auxiliary circuit is transferred to the output during this time. The current through L_{r1} and L_{r2} decreases and goes to zero. The currents through S_1 and S_2 then become negative and flow through their body diodes. When this happens, S_1 can be turned off with ZCS.

In deriving the equation of this mode, it should be noted that because S_a has to be turned off right after turning off the main switches, the ZCS condition for main and auxiliary switches must be met in this mode of operation. The modal equations are as follows:

$$-V_{Cr}\,(t_3) + L_{r2}C_r \frac{di_{lr2}}{dt}\,(t_3) = 0 \tag{10}$$

$$-V_X - V_{Cr(t_3)} - L_{r1} \frac{di_{lr1}}{dt}\,(t_3) = 0 \tag{11}$$

$$i_{lr1}\,(t_3) = i_{cr}\,(t_3) + i_{lr2}\,(t_3) \tag{12}$$

$$i_{Cr}\,(t_3) = C_r \frac{dV_{Cr}}{dt}\,(t_3) \tag{13}$$

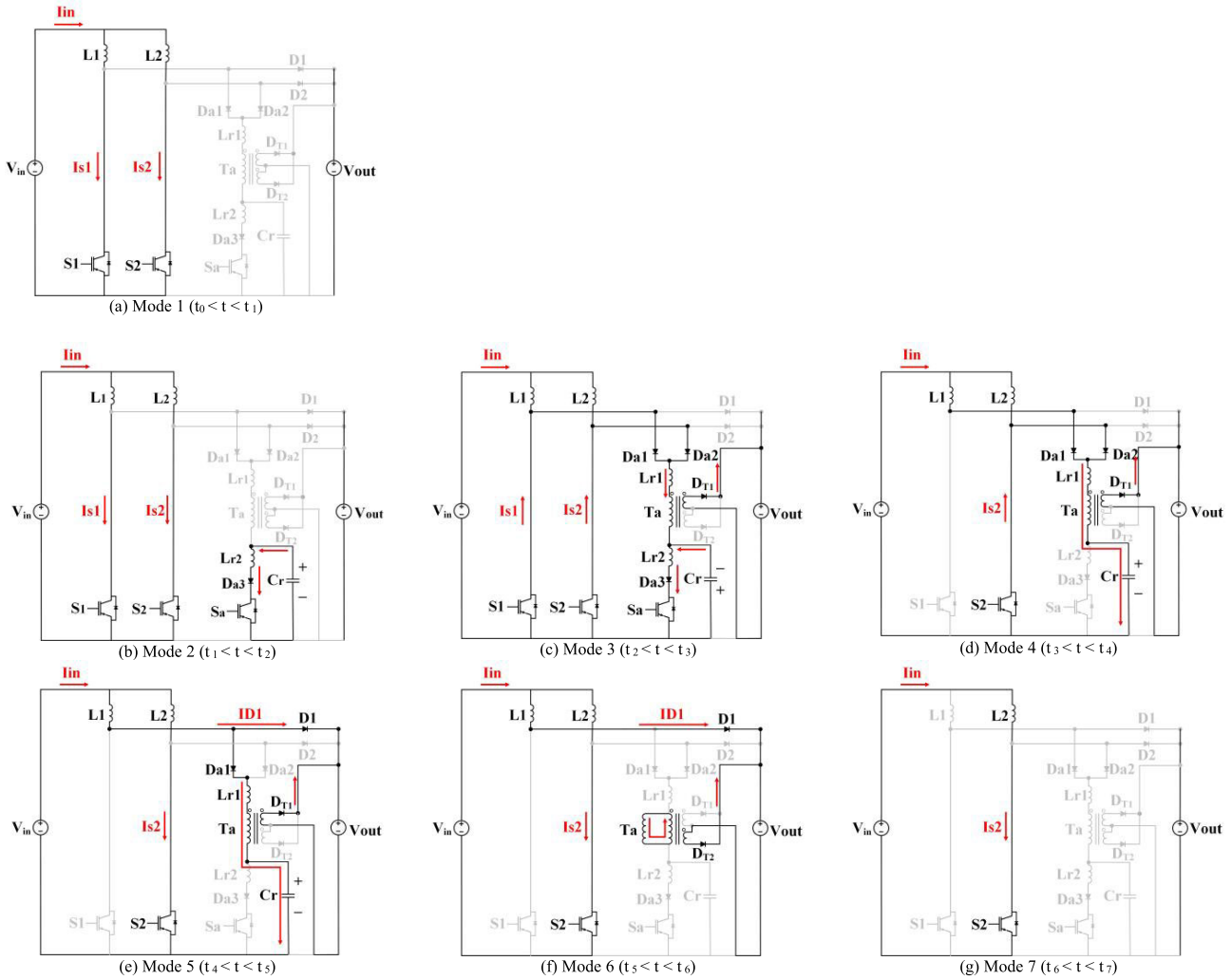

(a) Mode 1 ($t_0 < t < t_1$)

(b) Mode 2 ($t_1 < t < t_2$)

(c) Mode 3 ($t_2 < t < t_3$)

(d) Mode 4 ($t_3 < t < t_4$)

(e) Mode 5 ($t_4 < t < t_5$)

(f) Mode 6 ($t_5 < t < t_6$)

(g) Mode 7 ($t_6 < t < t_7$)

FIGURE 3. **Modes of operation.**

The transformer primary is clamped to $V_X = V_o/N$ where $N = N_2/N_1$ is the turn ratio.

$$-\frac{d^2V_{Cr}\,(t_3)}{dt^2} - \frac{V_{Cr}}{L_eC_r}\,(t_3) - \frac{V_X}{L_{r1}C_r} = 0 \tag{14}$$

$$\frac{di_{lr1}}{dt}\,(t_3) = -\frac{(V_{Cr}\,(t_3) + V_X)}{L_{r1}} \tag{15}$$

Solving these equations gives (16)-(18), as shown at the bottom of the next page, where:

$$\omega_1 = \frac{1}{\sqrt{L_{r1}C_r}},\quad \omega_e = \frac{1}{\sqrt{L_eC_r}}\quad Z_1 = \sqrt{\frac{L_{r1}}{C_r}},$$

$$Z_e = \sqrt{\frac{L_{re}}{C_r}}\ and\ L_e = \frac{L_{r1} * L_{r2}}{L_{r1} + L_{r2}}.$$

During this mode the current in L_{r2} reaches zero because of its resonance with C_r; then energy in L_{r1} is transferred to C_r, thus increasing its voltage so that V_{Cr} becomes less negative and is in the process of eventually becoming positive. When the (18-a) and (18-b) are zero or negative, the ZCS for the main and auxiliary switches is maintained, respectively. The operation time of Mode 3 is shown in (19), at the bottom of the next page. By simplifying the equations, the operation time of the auxiliary switch to perform ZCS for itself and the main switches can be calculated by (20).

The maximum voltage of the resonant capacitor, which is the maximum voltage across the auxiliary switch V_{cm}, should be derived in Modes $4-5$. Due to page limitations, only the last formula will be presented. The procedure is the same as for the previous equations.

Mode 4 ($t_3 < t < t_4$): This mode begins when S_a is turned off with ZCS. The voltage across the V_{cr} keeps increasing. So, the current through the S_2 starts to be less negative. The negative current through body diode of S_2 decrease to zero, thus auxiliary diode D_{a2} stops conducting at the end of this mode.

Mode 5 ($t_4 < t < t_5$): This mode begins when the net voltage across the C_r and L_{r1} becomes positive, thus D_1

conducts. This mode ends when the current through the L_{r1} reaches zero. At the end of this mode, the maximum voltage across the auxiliary capacitor V_{cm} can be derived by (21).

Mode 6 ($t_5 < t < t_6$): This mode begins when I_{Lr1} reaches to zero thus D_{a1} and D_{T1} stop conducting. During this mode, the current in the magnetizing inductance of the feed forward transformer is discharged to the output by the D_{T2}. The voltage across L_1 becomes ($V_{in,rec} - V_o$) and the current through L_1 starts to decrease linearly.

$$V_{Cr}(t_3) = \frac{\left(V_X w_1^2\right)(\cos(w_e t_3) - 1)}{w_e^2} - \frac{(V_{Cm} Z_e)(\sin(w_e t_3))}{Z_2} \tag{16}$$

$$i_{Lr1}(t_3) = \frac{(V_{Cm} L_e)(1 - \cos(w_e t_3))}{Z_2 L_{r1}} + \frac{(V_X L_e)\left(t_3 - \frac{\sin(w_e t_3)}{w_e}\right)}{L_{r1}^2} - \frac{V_X t_3}{L_{r1}} \tag{17}$$

$$t_{isa-ontime} = 2\left(\frac{\pi - tan^{-1}\left(\frac{V_{cm} w_e^2 Z_e}{V_X w_1^2 Z_2}\right)}{w_e}\right) \tag{20}$$

$$V_{Cr}(t_6) = V_{Cm} = \left(V_{Cr_6}(0) + V_X - V_O\right)(\cos(w_1 t_6)) + \frac{i_{lr1_6}(0)(\sin(w_1 t_6))}{c_r w_1} - V_X + V_0 \tag{21}$$

Mode 7 ($t_6 < t < t_7$): This mode begins when the current in L_1 reaches zero. This is the last mode of the half- cycle. The next half-cycle begins when S_1 is turned on under ZCS.

III. DESIGN PROCEDURE AND EXAMPLE

The modal equations derived in Section II can be used solved and then used to as part of a computer program to generate steady-state characteristic curves of possible converter operating points that can be used as part of a design procedure. Due to limitations on paper size, only some example equations were shown on the previous section to prove the soft switching. These equations can then be used to develop a computer program that can be used to determine to generate graphs of steady-state characteristics. This can be done as shown in [39]. with these graphs, a procedure for the design of the auxiliary circuit converter can then be developed.

The design procedure that is presented here is iterative and requires several iterations before the final design can be completed. Only the final iteration will be shown in the example that follows. The key auxiliary circuit components that should be designed are the the resonant capacitor C_r. the two auxiliary circuit inductors L_{r1} and L_{r2}, and the transformer turns ratio.

The key circuit voltages that need to be considered are the output voltage $V_0 = 400$ V and the worst-case input voltage. This input voltage is the voltage at which maximum current flows through the converter, which is the minimum input voltage $V_{in} = 8\ 5$ V. Based on (18_a), if the auxiliary circuit can be designed to maintain ZCS under worst-case conditions with minimum input voltage and maximum load, then it can operate under all other conditions. The maximum input current, assuming a targeted efficiency of 95% is

$$i_{in,max} = \frac{\sqrt{2} P_o}{\eta V_{in}} \rightarrow \frac{\sqrt{2} * 1000}{0.95 * 85} = 17.5\ A \tag{22}$$

It should be noted that to maintain ZCS for the main switches, the value of the maximum current through the auxiliary switch should be higher than that of the input current. In order to ensure ZCS operation of the main switches, a potential maximum current of 17.5 A may need to be diverted away from these switches. This means that a current of at least 17.5 A must be allowed to flow in the auxiliary switch. To fully ensure ZCS operation, the current that can flow in the auxiliary switch should be more than this. Assuming a conservative 20% - 30% margin, the converter can be designed to ensure that the auxiliary switch conducts 22 A of current and thus (7) can be rewritten as

$$i_{sa,max} = \frac{V_{cm}}{Z_2} > i_{in,max} \tag{23}$$

$$i_{samax} = \frac{V_{cm}}{Z_2} = 22\ A \tag{24}$$

$$i_{S1,2}(t_3) = i_{in} - \left(\frac{(V_{Cm} L_e)(1 - \cos(w_e t_3))}{Z_2 L_{r1}} + \frac{(V_X L_e)\left(t_3 - \frac{\sin(w_e t_3)}{w_e}\right)}{L_{r1}^2} - \frac{V_X t_3}{L_{r1}}\right) \tag{18_a}$$

$$i_{Sa}(t_3) = i_{Lr2}(t_3) = \frac{V_{cm}}{Z_2} - \left(\frac{(V_{Cm} L_e)(1 - \cos(w_e t_3))}{Z_2 L_{r2}} + \frac{\left(V_X w_1^2\right)\left(t_3 - \frac{\sin(w_e t_3)}{w_e}\right)}{L_{r2} w_e^2}\right) \tag{18_b}$$

$$t_3 = -\frac{\log\left(\frac{\sqrt{\left(\frac{V_X L_e}{L_{r1}^2} - \frac{V_X}{L_{r1}}\right) j + \left(\left(\frac{V_{cm} L_e}{Z_2 L_{r1}}\right)^2 w_e^2 + \left(\frac{V_X L_e}{L_{r1}^2}\right)^2 - \left(\frac{V_X L_e}{L_{r1}^2} - \frac{V_X}{L_{r1}}\right)^2\right)}}{\frac{V_X L_e}{L_{r1}^2} j - \frac{V_{cm} L_e}{Z_2 L_{r1}} w_e}\right) j}{w_e} \tag{19}$$

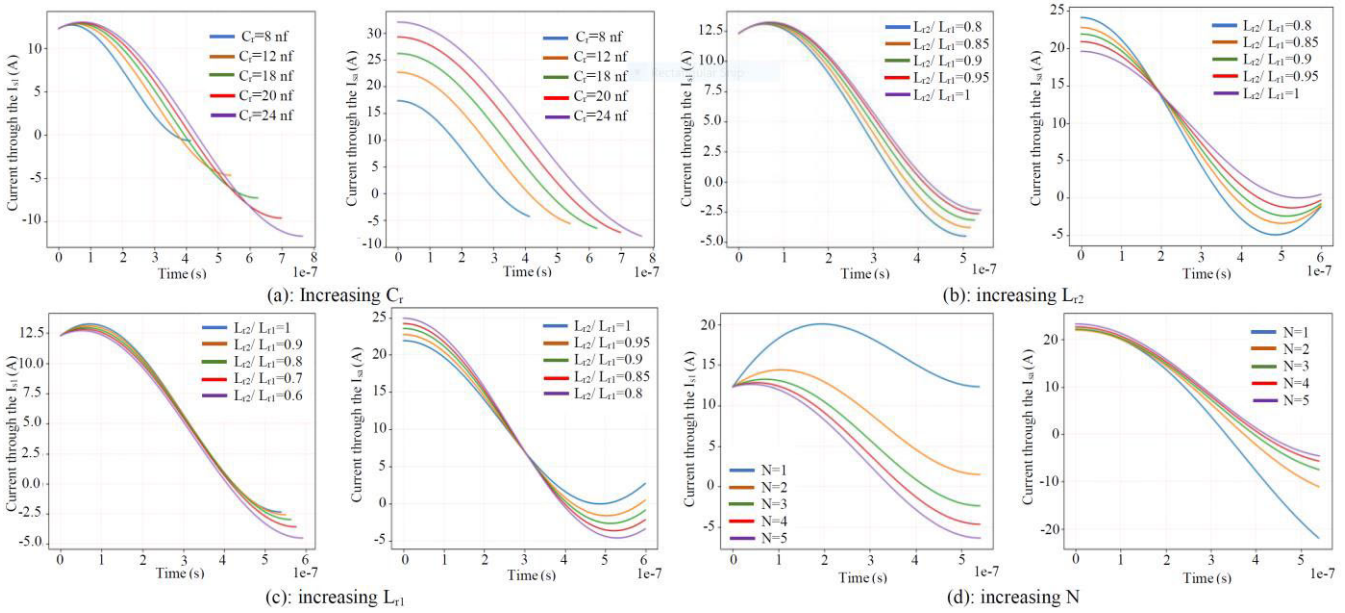

FIGURE 4. Effects of increasing the key parameters on the ZCS conditions for main and auxiliary switches.

A. RESONANT CAPACITOR (C_r)

In order to have less voltage stress on the auxiliary switch, V_{cr}, which is also the peak auxiliary switch voltage is designed to be approximately 450 V, (21), to take into account the fact that the auxiliary switch is not directly connected across the anode of a boost diode and ground. It should be noted that this voltage would be much higher if there was no transformer T_a to help transfer energy to the output [25], [29]–[31].

Fig. 4 shows graphs of main switch current vs time and auxiliary switch current vs time for various parameters. Fig. 4(a) shows graphs for main switch current vs time and auxiliary switch current vs time with fixed values of L_{r1}, L_{r2}, and N and varying C_r. Fig. 4(b) shows these two graphs with fixed values of C_r, L_{r1}, and N with varying values of L_{r2}. Fig. 4(c) shows the graphs with fixed values of C_r, L_{r2}, and N and varying values of L_{r1}. Fig. 4(d) shows the graphs with fixed values of C_r, L_{r2}, and L_{r1} and with varying values of N. Each of the graphs in Fig. 4 is drawn with the start of Mode 3 as $t = 0$; this is when current begins to be diverted from the main switch after the auxiliary switch has been turned on, which happens during Mode 2. For all the curves in the graphs, current falls after $t = 0$. If a current curve in these graphs reach zero or becomes negative, this is an indication of ZCS because this means that the current in the switch can be removed and/or current can flow in the body-diode of the switch device. If a current curve cannot reach zero, this is an indication that current cannot be fully removed from a switch so that that switch cannot turn off with ZCS.

In Fig. 4(a) it can be seen that by decreasing the value of the resonant capacitor C_r, the maximum current through the auxiliary switch is decreased, but the ZCS condition of the main switches is lost as the current cannot fall to zero.

C_r should impose a negative voltage across resonant inductor L_{r2} after S_a is turned on to allow current to be transferred away from either S_1 or S_2 before a turn-off occurs to ensure that it can be done with ZCS. A negative C_r voltage allows current to be diverted away from a main switch to C_r. C_r should be large enough to ensure that its voltage does not become positive as this transfer of current is taking place, but not too large as this will force the auxiliary switch to be on for a longer time, thus increasing its losses.

According to Fig. 4(a), C_r should be more than 8 nf in order to ensure that the main switches and the auxiliary switch can turn on with ZCS – the main switches will not be able to turn on with ZCS if C_r is less than 8 nf. C_r, however, should not be too large as this would increase peak current stress and slow down the transfer of current away from the auxiliary switch, which would require that the auxiliary switch be on longer and thus increase RMS current stress and conduction losses. In order to have a margin for ZCS and maintain the maximum current through the auxiliary switch between 18-22 Amps, C_r is chosen to be 12 nf.

B. RESONANT INDUCTOR (L_{r2})

With a value of C_r chosen and the maximum auxiliary switch current set to be 22 A as described at the start of this section, a value of L_{r2} can be determined as follows:

$$i_{samax} = \frac{V_{cm}}{Z_2} = \frac{V_{cm}}{\sqrt{\frac{L_{r2}}{C_r}}} = 22\ A \tag{25}$$

$$22 = \frac{450}{\sqrt{\frac{L_{r2}}{12e{-}9}}} \rightarrow L_{r2} = 4.9\ \mu H \tag{26}$$

This value of L_{r2} is a preliminary value that can only be set in conjunction with L_{r1}, as will be described next.

C. RESONANT INDUCTOR L_{r1}

The choice of L_{r1} can be made by using the graphs of L_{r2}/L_{r1} in Figs 4(b) and 4(c). As can be seen from Fig. 4(b), the ratio of L_{r2}/L_{r1} should be small enough to minimize the time that the auxiliary switch is on to reduce RMS switch current stress and conduction losses. It should, however, also be large enough to reduce auxiliary peak current. Based on the characteristic curves in Fig. 4(c), the value of L_{r1} should be greater than that of L_{r2} because the current through L_{r1} should be less than current through L_{r2} in Mode 3 of operation to divert the current from the auxiliary circuit and turn it off with ZCS. In other words, L_{r2}/L_{r1} should be less than 1 because the auxiliary switch will not be able to turn off with ZCS. L_{r2}/L_{r1} should not be too small, however, as the maximum current through the auxiliary switch is increased. As a result, a ratio of $L_{r2}/L_{r1} = 0.95$ is chosen to have lower peak current, but with ZCS. With ratio and $L_{r2} = 4.9$ uH, L_{r1} can be set to be 5.15 uH.

$$L_{r1} > L_{r2} \rightarrow L_{r1} = 5.5\ \mu H \tag{27}$$

D. TRANSFORMER (T_a) TURN RATIO (N)

The value of N, defined as the ratio of N_2/N_1, cannot be too large or too small as the converter switches will not be able to operate with ZCS in either case. As shown in Fig. 4(d), by increasing the value of N, the ability of the auxiliary switch to turn off with ZCS is reduced as the current in the switch becomes less likely to fall to zero. According to Fig. 4(d), the auxiliary switch cannot be turned off with ZCS if $N > 5$. On the other hand, if too small a value of N is chosen (e.g. $N < 3$), the ZCS condition for the main switches will be lost because if N is too small, then the counter voltage produced at the transformer's primary will be too high and will counteract the voltage across C_r to such an extent that the full switch current will not be diverted from the main switch. As a result, the value of N should be between 3 and 5.

Fig. 5 shows the power that the transformer transfers to the load for different turn ratios. It can be seen from this graph that as N is decreased, the transformer must handle more power and thus must be made larger. As a result, if the range of N that allows the converter switches to operate with ZCS is between 3 and 5, then a value of $N = 5$ should be chosen to minimize the amount of power that the transformer must handle and thus its size.

E. OPERATING TIME OF THE AUXILIARY SWITCH

The time that the auxiliary switch operates which is the time it needs to perform ZCS for itself and the main switches was derived in (20). By substituting the values of the parameters that has been chosen in this section: $l_{r1} = 5.15$ uH, $L_{r2} = 4.9\ \mu$H, $N = 5$, $C_r = 12$ nF, and the $V_{cm} = 450$, the time that the auxiliary switch needs to perform ZCS for main switches and itself is equal to 0.6 μs.

$$t_{isa-ontime} = 2 * \frac{\pi - tan^{-1}\left(\frac{450 w_e^2 Z_e}{V_X w_1^2 Z_2}\right)}{w_e} \tag{28}$$

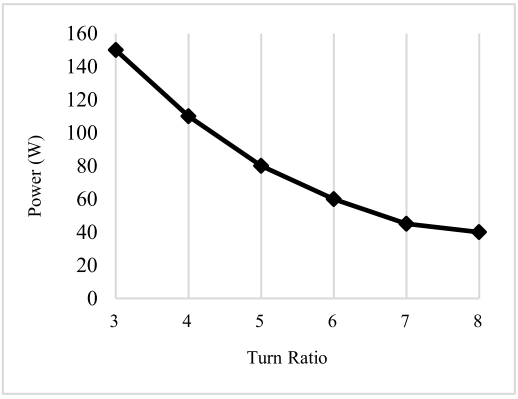

FIGURE 5. Auxiliary transformer power vs turn ratio.

IV. COMPARISON OF POWER LOSSES

The key power losses of the converter are discussed in this section; just the key power losses are covered to simplify the discussion. The loss analysis of the proposed converter is made based on three main sources of losses: conduction losses, switching losses and transformer losses. In addition, a comparison is made for the proposed converter when it works with ZCS and without ZCS.

There are three main sources of conduction losses in the proposed converter: power losses in IGBT devices, power losses in diodes (e.g. device body diodes, output and auxiliary diodes), and transformer winding losses. Switching losses will be considered only when the converter is operating without ZCS. More details will be explained as follows:

A. CONDUCTION LOSSES OF THE IGBT TRANSISTORS

In the proposed converter there are two main switches and one auxiliary switch and the power dissipation when current is flowing through the IGBT switches can be determined using

$$P_c = \frac{1}{T_s}\int_0^{T_s} P_c\,(t)\,dt = v_{CE0} I_{savg} + r_c I_{srms}^2 \tag{29}$$

where, T_s is the switching cycle, V_{ceo} is the collector-emitter saturation voltage, r_c is the collector resistor when the transistor is turned on, I_{savg} is the collector average current and I_{srms} is the collector-rms current. The conduction losses of the main switches $S_1 - S_2$ can be determined by

$$P_{c\_m} = 2(v_{CE0} I_{sm\_avg} + r_c I_{sm\_rms}^2) \tag{30}$$

I_{sm_avg} and I_{sm_rms} can be determined by integrating the current waveform of each main switch in DCM operation for a conventional boost converter as follows:

$$I_{sm\_avg} = \left(\frac{V_{in} D_1}{L_{in} f_s}\right)\left(\frac{D_1}{2}\right) \tag{31}$$

$$I_{sm\_rms} = \left(\frac{V_{in} D_1}{L_{in} f_s}\right)\sqrt{\frac{D_1}{3}} \tag{32}$$

where V_{in} is the input voltage, L_{in} is the input inductor for one leg, D_1 is the duty cycle during on time, f_s is the switching

frequency for main switch, and v_{co} and r_c can be determined by the transistor specifications.

The other conduction loss is the power loss in the auxiliary switch S_a, and it can be determined by using

$$P_{c\_a} = v_{CE0} I_{sa\_avg} + r_c I^2_{sa\_rms} \tag{33}$$

I_{sa_avg} and I_{sa_rms} are the average and rms collector currents for the auxiliary switch and they can be calculated by using Fig. 2 as follows:

$$I_{sa\_ang} = \frac{1}{T_s}\left(\int_{t_1}^{t_2} i_{sa}(t)\,dt + \int_{t_2}^{t_3} i_{sa}(t)\,dt\right) \tag{34}$$

$$I_{sa_{rms}} = \sqrt{\frac{1}{T_s}\left(\int_{t_1}^{t_2} i^2_{sa}(t)\,dt + \int_{t_2}^{t_3} i^2_{sa}(t)\,dt\right)} \tag{35}$$

It should be noted that current i_{sa} during time $(t_1 - t_2)$ is determined by (6) and current i_{sa} during time $t_2 - t_3$ is determined by (18-b).

B. CONDUCTION LOSSES OF THE DIODES

The power dissipation when current is flowing through the body diodes of the converter switches and through the output and auxiliary diodes can be determined by multiplying the average value of the current, I_{Favg}, with the forward voltage drop, V_F, as follows:

$$P_{CD} = V_F I_{Favg} \tag{36}$$

In the proposed converter, the body diodes of the IGBTs devices conduct for very small time, thus, the conduction losses in these diodes will be neglected in this analysis. The total conduction losses of the diodes in the proposed converter is

$$P_{C\_D} = 2\left(V_{F_{D1}} I_{Favg_{D1}}\right) + 2\left(V_{F_{Da1}} I_{Fav_{Da1}}\right) V_{F_{Da3}} I_{Fav_{Da3}} + V_{F_{DT1}} I_{Fav_{DT1}} + V_{F_{DT2}} I_{Fav_{DT2}} \tag{37}$$

C. TRANSFORMER LOSSES

Two kinds of transformer losses will be considered in this analysis: core loss and copper (winding) loss. The core loss depends on the size of the transformer thus the transformers size will be selected first. The core size of the transformers in the proposed converter can be selected by using

$$A_P = \frac{P_t(10^4)}{K_f K_u B_m J f_{sw}} \tag{38}$$

where A_p is the area product, B_m is the density, J is the current density, K_u is the window utilization factor, K_f is the waveform coefficient, f_{sw} is the switching frequency, and P_t is the transformer apparent power. In this design ETD 29 is selected to be the cores of auxiliary transformer. The transformer core losses can be estimated from the manufacturer's datasheet and the transformers ohmic losses can be estimated as:

$$P_{wind-Tr} = \left(R_{pri} I^2_{prms} + R_{sec} I^2_{srms}\right) \tag{39}$$

where, R_{pri} and R_{sec} are the primary and secondary winding resistances for the auxiliary transformer respectively, I_{prms} and I_{srms} are the rms primary and secondary currents for the auxiliary transformer, respectively.

D. SWITCHING LOSSES

During a switching transition, there is an overlap between the voltage across the switch and the current flowing through it and it is this overlap of voltage and current that creates the losses. Switching losses of IGBTs devices in the proposed converter when it works without the auxiliary circuit will be considered in this analysis as there are no switching losses when the auxiliary circuit is engaged. There are two types of switching losses: turn-on losses and turn-off losses. The switching losses for one of the main switches is represented as:

$$P_{sw} = (E_{on} + E_{off}) f_{sw} \tag{40}$$

where E_{on} is turn-on energy, E_{off} is turn-off energy and f_{sw} is switching frequency.

Since the proposed converter works under DCM mode of operation, the turn-on losses will not be considered as the switches turn on with ZCS. In other words, the proposed converter only has turn-off losses when it works without the auxiliary circuit, which are the dominant losses in the IGBTs. The turn-off losses can be calculated as follows:

$$P_{sw} = \left[\left(A_{off} I_c + B_{off}\right) Z\right] f_{sw} \tag{41}$$

$$Z = \frac{E_{off(R_{guser})}}{E_{off(R_{gdatasheet})}} \frac{V_{DCoff(user)}}{V_{DCoff(datasheet)}} \frac{E_{off(T_j)}}{E_{off(T_{jmax})}} \tag{42}$$

where, A_{off} and B_{off} are parameters that can be calculated using the datasheet of the IGBT transistor as in [41], I_c is the collector current when the switch is turned off. Since the gate resistor of the gate drive used in this article does not have the same value as the gate resistor in the test circuit specified in the datasheet, the actual values related to the gate drive are considered. $E_{off(Rguser)}$ is the turn-off energy at used gate resistor, $E_{off(Rgdatasheet)}$ is the turn-off energy in datasheet, $V_{DCoff(user)}$ is the actual collector voltage when the switch is turned off, $V_{DCoff(datasheet)}$ is the collector voltage in the datasheet, $E_{off(Tj)}$ is the turn-off energy at the operating temperature, and $E_{off(Tjmax)}$ is the turn-off energy at maximum temperature.

E. POWER LOSS COMPARISON

In this section, a loss comparison between the proposed converter operating with and without the auxiliary circuit (conventional interleaved converter) is presented.

The comparison is made at full load and 20% of rated power based on different power losses: conduction of the switches (PC_S), switching (Poff), conduction of the diodes (PC_D), transformer (PTr), and other losses. The power loss breakdown for each converter is shown in Fig. 6.

As can be seen, at light load, the hard-switching converter is more efficient, while at rated power, the proposed soft-switching converter has considerably better efficiency than the standard converter. Since the proposed converter has the

capability to operate with hard-switching at light loads and operate with soft switching at heavier loads, high converter efficiency can be maintained throughout the load range.

V. CONVERTER FEATURE

The features of the proposed converter are reviewed in this section. The features that are discussed in this section address the eight drawbacks that are stated in the Introduction of this article.

(a) The proposed converter has only one auxiliary circuit that helps the main switch in both modules turn off with ZCS. Although this circuit may seem complicated, the number of passive elements in the circuit is comparable to that of two previously proposed active circuits in many cases, and there is just one active switch instead of two.

(b) There is no auxiliary circuit component in the main current path so that less expensive, lower current and power rated devices can be used as auxiliary circuit components.

(c) The auxiliary circuit does not inject current into the main converter switches, as is the case with resonant-type auxiliary circuits in other ZCS-PWM converters as there is a blocking diode for each module that prevents the auxiliary circuit from doing so. This makes the current stresses of the main switches the same as those of the main switches of a hard-switched PWM boost converter.

(d) The auxiliary switch has a ZCS turn-on because inductor L_{r2}, limits the rise of current that starts to flow through it when it is turned on and a ZCS turn-off as described in Mode 3 of Section II.

(e) If desired, the auxiliary circuit does not have to be used when the converter is operating under light-load conditions. This is unlike many ZCS-PWM converter that require the auxiliary circuit to be used even under light-load conditions where it is actually detrimental as there are components in the main part of the circuit. This helps improve light-load efficiency.

(f) Energy that is pumped into the auxiliary circuit is not trapped inside it as the auxiliary circuit transformer provides a mechanism by which some of it can be removed through diodes D_{T1} and D_{T2}. Without the transformer, energy that is pumped into the auxiliary circuit from the main modules would have to be dissipated in the auxiliary circuit, which could create losses.

(g) The boost diode in each module has a lower peak voltage stress that that found in other previously proposed ZCS-PWM converter with resonant auxiliary circuits as the auxiliary circuit transformer makes the voltage of the anode less negative since it provides a counter-voltage to the voltage across resonant capacitor C_r. For example, in [24], which has a transformer in its auxiliary circuit, the transformer does not provide such a counter voltage, thus the peak voltage stress on the boost diode can be 1.6-1.7 times the output voltage.

(h) The RMS current stress of the auxiliary switch is significantly less than that found in other ZCS-PWM converters. This allows the auxiliary circuit to be implemented in a two-module interleaved boost converter and be used to assist both main converter switches turn off with ZCS and do so while allowing the converter to operate at a higher power level than that of other previously proposed interleaved ZCS-PWM converters.

A more detailed explanation of this final feature is given here. In ZCS-PWM converters, current must be gradually diverted away from the main switch in order for it to able to turn-off with ZCS. If the transfer is performed too quickly, the main switch IGBT device will not have a soft turn-off due to residual charge in the device. In converters where a snubber capacitor is connected across the main switch/series inductor, the snubber capacitor voltage can swing to as high as $-V_o$. If this voltage swing from V_o to $-V_o$ is too fast, then the current diversion away from the main switch will be too fast as well. As a result, this voltage swing needs to occur gradually, which means that the snubber capacitor needs to be discharged gradually so that the auxiliary switch must conduct current for some time (but not as long as the main switch) in order for the main switch to turn off with ZCS.

In the proposed converter, since the transformer in the auxiliary circuit in placed in series with capacitor C_r where it is like a counter positive voltage source, the current transfer will automatically be more gradual as the net voltage across L_{r1} is reduced. Capacitor C_r can thus be discharged more quickly, so that the polarity of its voltage does swing to negative (which allows current to be diverted away from a main switch), but the counter voltage produced by T_a prevents this capacitor from then being charged too quickly so that the time window for ZCS is lost. As a result, the auxiliary switch in the proposed converter does not have to stay for as long as the auxiliary switch in other ZCS-PWM converters as it can be used just to quickly C_r. RMS current stress is lower and cheaper and lower current-rated device can be used as the auxiliary switch. Even more important, given the fact that the auxiliary switch is activated twice during a switching cycle, as stated in the Introduction, it allows the proposed multi-module converter to operate at higher power levels with one auxiliary switch than other previous proposed interleaved multi-module ZCS-PWM converters that that have just one auxiliary switch.

Table 1 shows a list of previously proposed ZCS-PWM converters that use auxiliary switch to perform ZCS. The key things to note from this table are as follows:

- Table 1 includes references of ZCS-PWM converters that consist of just one module are non-interleaved. This is to examine whether these converters can be adapted to two-module interleaved converters.
- The proposed converter is the only converter that has all the eight features that are discussed in this section.

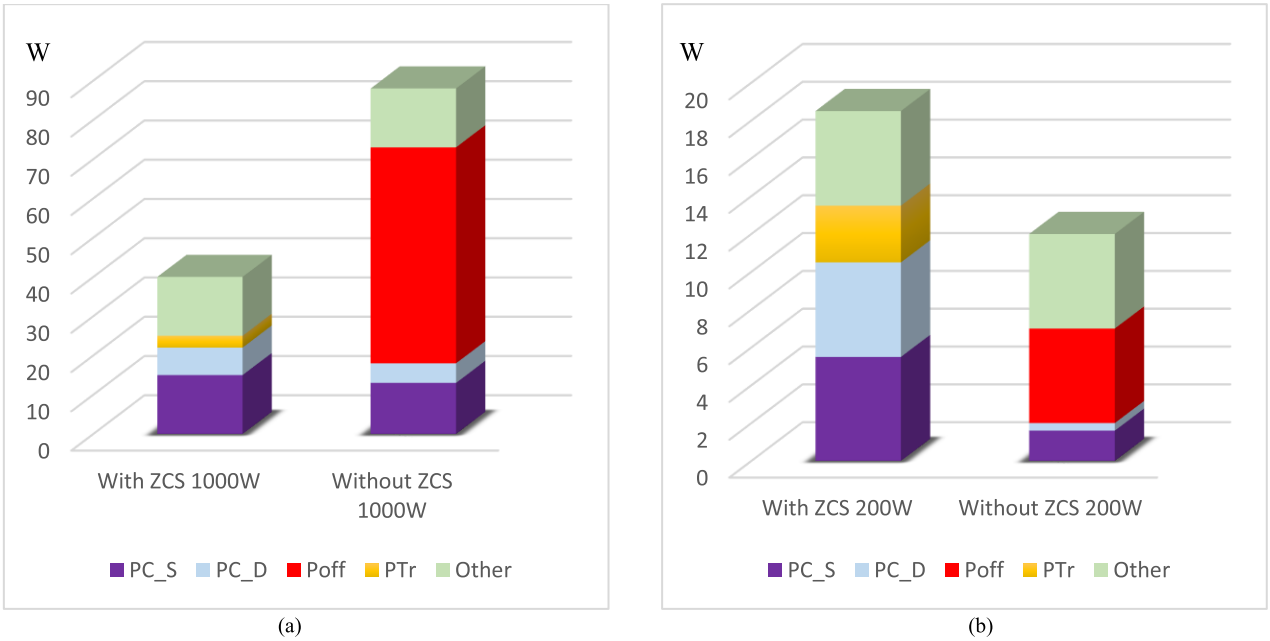

FIGURE 6. Loss comparison for the proposed converter and the converter without ZCS. (a) rated load, (b) 20% load.

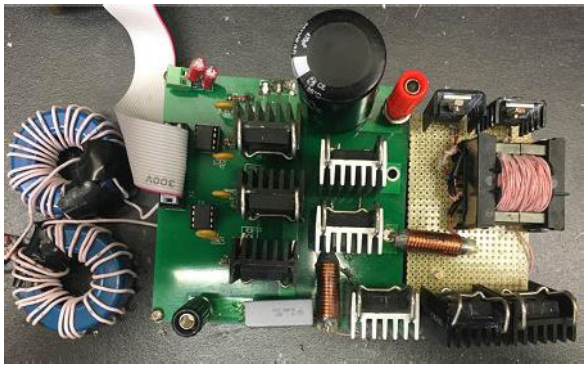

FIGURE 7. Prototype picture.

- The on-time of the auxiliary switch after it has been activated is much less than that of almost all the other converters, as can be seen in the one before the last column. With some of the other converters, this on-time is so long, that the auxiliary circuit must handle a considerable amount of power. If lower power-rated components are used in the auxiliary circuit, this places limitations on the power that the converter can operate with, as can be seen in the last column. It should be noted that non-interleaved ZCS-PWM converters cannot be adapted for use in ZCS-PWM interleaved converters if the auxiliary switch on-time is significant.

VI. EXPERIMENTAL RESULTS

A prototype of the proposed converter was built to confirm its feasibility. The prototype was built with the following specifications as indicated at Table 2: Input voltage V_{in} = 85-265 V_{rms}, output voltage V_o = 400 V_{dc}, switching frequency f_{sw} = 50 kHz, maximum output power $P_{o,max}$ = 1 kW. The picture of the prototype, which is a simple proof-of-concept prototype, is shown in Fig.7 and the experimental results are shown in Fig.8.

Fig. 8(a) shows typical input voltage and input current waveforms. It can be seen that the input current is sinusoidal and input phase with the input voltage and that the input current is continuous. Fig. 8(b) shows current waveforms for input boost inductors L_1 and L_2. It can be seen that these currents are discontinuous and identical. Fig. 8(c) shows the interleaved current that is a sum of the current in L_1 and L_2.

Fig. 8(d) shows typical current and gating signal waveforms for one of the main switches. It can be seen that the switch can be turned on with ZCS and can be turned off with ZCS, without a current tail, because the current through the switch goes to zero before turning it off. The same waveforms are shown in Fig. 8(e) for the auxiliary switch and it can be seen that the auxiliary switch turns on and off with ZCS as well. Fig. 8(f) shows the voltage and the current of one of the main boost diodes where the maximum voltage of the diode is clamped to the output voltage which is 400 V. Fig. 8(g) shows the voltage across the auxiliary capacitor which is less than 450 V as discussed in the design procedure.

It should be noted that there is some voltage oscillation in the waveforms of Fig. 8(d) and 8(f) when one of the main switches is turned on. This oscillation is caused by interaction of the input inductor and the output capacitance of the main switch in a module This phenomenon arises when the input inductor current of a module is discontinuous. It has nothing to do with the proposed auxiliary circuit and can be found in any boost converter operating with a discontinuous input current. A full explanation of this phenomenon can be found in [35].

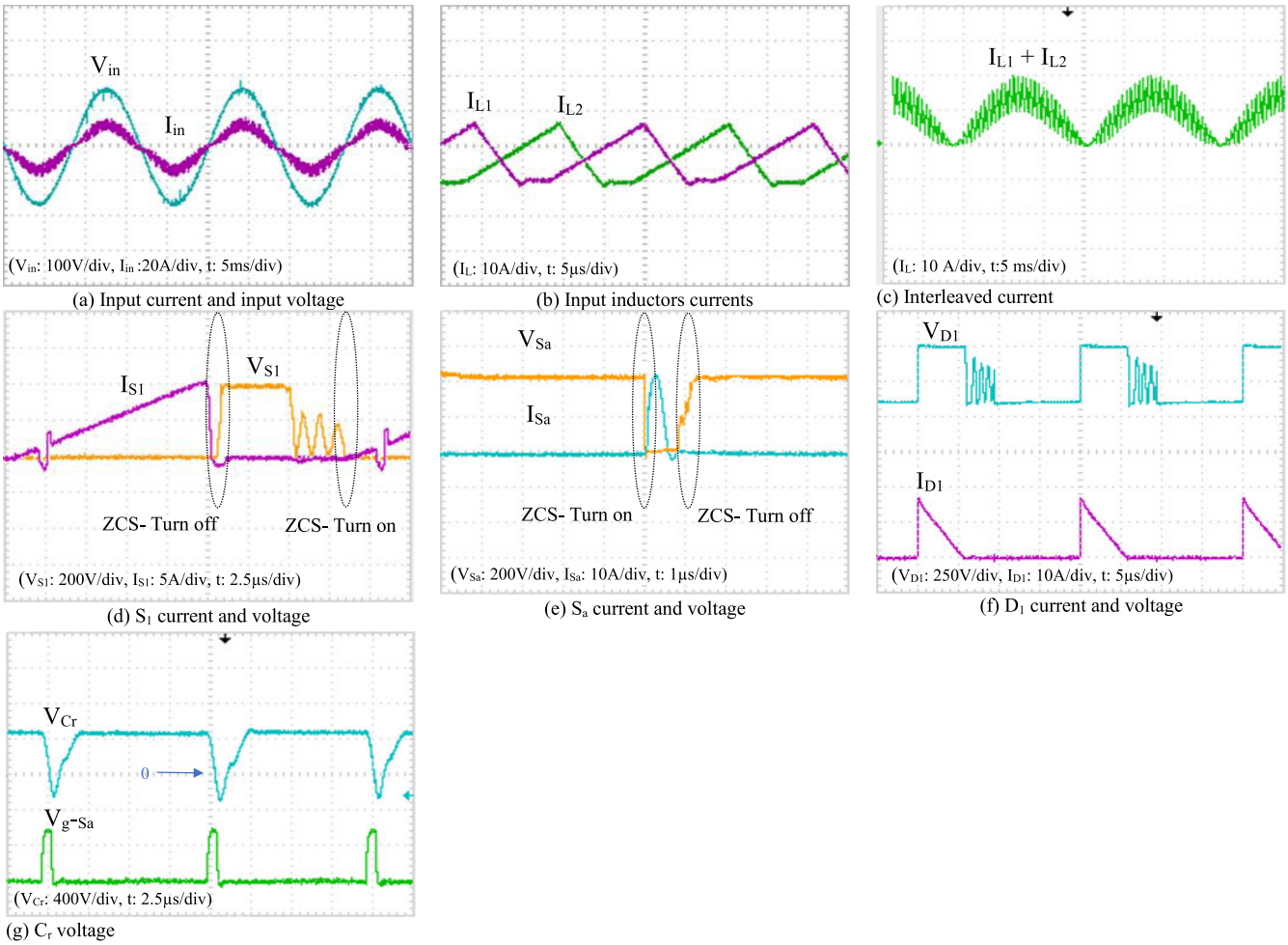

FIGURE 8. Experimental.

Eefficiency measurements show a maximum converter efficiency above 97% and an improvement in light-load efficiency by 7% when the auxiliary circuit is disengaged. Fig. 7 shows an efficiency comparison of the proposed ZCS-PWM interleaved boost converter and a conventional hard switching PWM interleaved boost converter. Both converters were implemented on the same prototype—one with the auxiliary circuit and one without.

As can be seen from Fig. 9, the efficiency of the conventional converter is decreased by increasing the load while the efficiency of the proposed converter is increased. The proposed converter has a significantly better efficiency than the conventional PWM boost converter above 40% of the full load, which is 1 kW, and that its efficiency is consistently about 95%.

The main reason for this, is that the auxiliary circuit losses dominate when the converter is operating under light loads.

Auxiliary circuit losses include the turning on and off of the auxiliary switch and additional conduction losses as there can be an increased amount of circulating current flowing in the converter. ZCS-PWM converters achieve their improved efficiency over hard-switching converters at heavier loads when switching losses of the main switches that are eliminated- especially the IGBT current tail losses - are greater than the auxiliary circuit losses. It should be noted that it is possible with the proposed converter to operate the converter with hard-switching when the converter is operating with light loads and with ZCS when it is operating with heavier loads, so that the converter can operate with ''maximum'' efficiency throughout the load range.

The proposed converter needs only one auxiliary circuit with just one active switch to help the two main converter switches turn off with ZCS. This auxiliary circuit does not need to be used when the converter is operating with light loads and its switch can be turned on or off with ZCS. None of its components are in the main path of current of any of the modules so that cheaper, lower current power rated devices can be used as auxiliary circuit components. Blocking diodes prevent the auxiliary circuit from injecting current into any of the main switches.

- The proposed converter has a transformer in its auxiliary circuit. This transformer allows energy that would otherwise be trapped in the auxiliary circuit to be transferred to the load.

TABLE 1. Comparison of ZCS-PWM converter features.

Reference	BC/IBC[1]	Features								$T_{aux\text{-}\mu s}$[2]	P_{kW}
		A	B	C	D	E	F	G	H		
[17]	IBC	✓	✓	✓	✗	✓	✗	✓	✗	3	0.6
[19]	IBC	✗	✓	✓	✓	✓	✗	✓	✗	3	1.2
[20]	IBC	✓	✗	✗	✓	✗	✗	✗	✗	1.5	0.5
[22]	IBC	✓	✗	✓	✓	✗	✗	✓	✗	14	0.25
[23]	IBC	✓	✗	✗	✓	✗	✗	✗	✗	2.5	0.25
[24]	BC	-	✗	✗	✓	✗	✓	✗	✗	2	1
[25]	IBC	✓	✗	✗	✓	✗	✓	✗	✗	7	1
[27]	BC	-	✗	✓	✓	✗	✗	✓	✗	0.6	0.3
[28]	IBC	✓	✗	✗	✓	✗	✗	✗	✗	0.6	0.2
[29]	IBC	✓	✗	✗	✓	✗	✓	✓	✗	1.5	0.12
[30]	BC	-	✗	✗	✓	✗	✓	✗	✗	16	0.7
[31]	IBC	✓	✗	✗	✓	✗	✓	✗	✗	0.6	0.5
[32]	BC	-	✗	✗	✓	✗	✓	✗	✗	10	1
[36]	BC	-	✗	✓	✓	✗	✓	✗	✗	4	2.5
[37]	BC	-	✗	✓	✓	✗	✓	✓	✗	8	0.25
[38]	BC	-	✗	✓	✓	✗	✓	✓	✗	4	0.5
Proposed Converter	IBC	✓	✓	✓	✓	✓	✓	✓	✓	0.6	1

[1] Interleaved boost converter (IBC) and regular single-module boost converter (BC).
[2] Auxiliary switch operation time in microseconds.

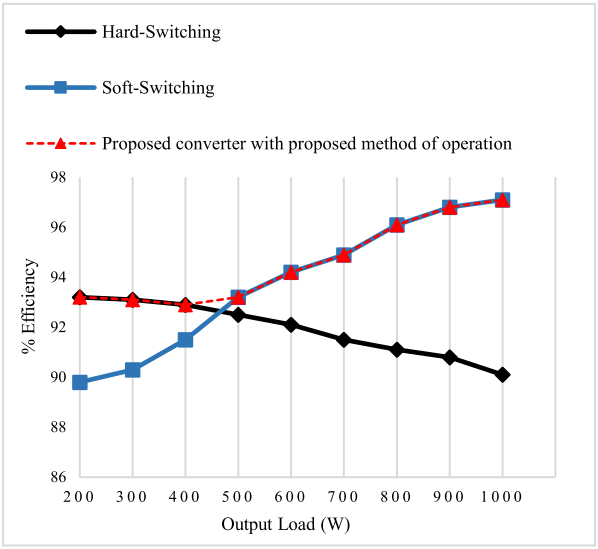

FIGURE 9. Interleaved boost converter efficiency with input voltage Vin = 85 V and output voltage V0 = 400 V.

TABLE 2. Specification of the converter components.

Symbol	Item	Value
V_{in}	Input voltage	85- 265 Volts
V_{out}	Output voltage	400 Volts
$P_{o,max}$	Maximum output power	1000 W
$P_{o,min}$	Minimum output power	200 W
$f_{sw,main}$	Main switches frequency	50 K HZ
$f_{sw,aux}$	Auxiliary switch frequency	100 K HZ
S_1,S_2	Main switches	K20H603
S_a	Auxiliary switch	K20H603
L_1, L_2	input inductors	120µH
C_o	Output capacitor	1000uF
D_1, D_2	Output diodes	40EPF06
D_{a1}, D_{a2}, D_{a3}	Auxiliary diodes	40EPF06
D_{T1}, D_{T2}	Output auxiliary diodes	LXA20T600
C_r	Auxiliary capacitor	12nf
L_{r1}	Auxiliary inductance	5.15 uH
L_{r2}	Auxiliary inductance	4.9 uH
n	The turn ratio of the auxiliary transformer	1:5:5

- Since there are no auxiliary components in the path of the main boost diodes, the peak voltage stress across them is clamped to the output voltage. This is significantly less than the $2V_o$ stress found in some other ZCS-PWM converters.
- The auxiliary circuit transformer helps reduce the RMS current stress of the auxiliary switch, as explained in SectII. Due to how the transformer is placed in the auxiliary circuit, the on-time of the auxiliary switch and thus its RMS current stress can be reduced significantly. For the proposed converter, on-time of 0.6 μs was used, which is much less than the on-time typically found in other ZCS-PWM converters.

To the best knowledge of the authors, no other presently existing ZCS-PWM interleaved boost converter has all these features.

It should also be mentioned that it is the existence of transformer T_a and its appropriate placement in the auxiliary circuit that allow the auxiliary switch to be implemented with an on-time that is lower than that of the auxiliary switch in other previously proposed interleaved ZCS-PWM boost converter. The transformer puts a counter-voltage in the resonant circuit path that slows down the transfer of current away from the main circuit module switches so that the auxiliary switch needs to be on for only a very short amount of time to quickly change the polarity of C_r. As a result, it becomes possible to implement an interleaved AC-DC boost converter with just one auxiliary circuit for heavier loads because the auxiliary switch will not have severe RMS stresses. This removes the need for a second auxiliary circuit, so that any increase in cost, size, and weight due to T_a is more than offset by the elimination of a second auxiliary circuit.

VII. CONCLUSION

A new AC-DC interleaved ZCS-PWM converter is proposed in this article. In the paper, its operating principles, modes of operation, and features were discussed. An analysis of the converter's steady-state operation was performed, and the results of the analysis were used to generate graphs of characteristic curves for various parameters that were then used to develop a design procedure. The design procedure was demonstrated with an example and the results of the example were used to implement a proof-of-concept experimental prototype that confirmed the feasibility of the converter.

REFERENCES

[1] J.-H. Kim, D. Y. Lee, H. S. Choi, and B. H. Cho, "High performance boost PFP (power factor pre-regulator) with an improved ZVT (zero voltage transition) converter," in *Proc. 16th Annu. IEEE Appl. Power Electron. Conf. Expo. (APEC)*, Mar. 2001, pp. 337–342.

[2] R. Pena-Alzola, M. A. Bianchi, and M. Ordonez, "Control design of a PFC with harmonic mitigation function for small hybrid AC/DC buildings," *IEEE Trans. Power Electron.*, vol. 31, no. 9, pp. 6607–6620, Sep. 2016.

[3] J. M. Galvez and M. Ordonez, "High performance boundary control of boost-derived PFCs: Natural switching surface derivation and properties," *IEEE Trans. Power Electron.*, vol. 27, no. 8, pp. 3807–3816, Aug. 2012.

[4] M. Ebrahimi and S. A. Khajehoddin, "Application of generalized peak current controllers for active power filters and rectifiers with power factor correction," in *Proc. IEEE Appl. Power Electron. Conf. Expo. (APEC)*, San Antonio, TX, USA, Mar. 2018, pp. 1316–1321.

[5] M. M. Hernando, A. Fernandez, J. Garcia, D. G. Lamar, and M. Rascon, "Comparing Si and SiC diode performance in commercial AC-to-DC rectifiers with power-factor correction," *IEEE Trans. Ind. Electron.*, vol. 53, no. 2, pp. 705–707, Apr. 2006.

[6] M. Arias, D. G. Lamar, F. F. Linera, D. Balocco, A. A. Diallo, and J. Sebastián, "Design of a soft-switching asymmetrical half-bridge converter as second stage of an LED driver for street lighting application," *IEEE Trans. Power Electron.*, vol. 27, no. 3, pp. 1608–1621, Mar. 2012.

[7] H. Valipour, M. Ordonez, and M. Mahdavi, "High-efficiency interleaved *LC* resonant boost topology: Analysis and design," *IEEE Trans. Power Electron.*, vol. 34, no. 11, pp. 10759–10775, Nov. 2019.

[8] R. Pena-Alzola, P. Ksiazek, M. Ordonez, H. Wang, and F. Blaabjerg, "Introducing state-trajectory control for the synchronous interleaved boost converter," in *Proc. IEEE Appl. Power Electron. Conf. Expo. (APEC)*, Mar. 2015, pp. 616–621.

[9] J. Zhu and A. Pratt, "Capacitor ripple current in an interleaved PFC converter," *IEEE Trans. Power Electron.*, vol. 24, no. 6, pp. 1506–1514, Jun. 2009.

[10] T. Nussbaumer, K. Raggl, and J. W. Kolar, "Design guidelines for interleaved single-phase boost PFC circuits," *IEEE Trans. Ind. Electron.*, vol. 56, no. 7, pp. 2559–2573, Jul. 2009.

[11] C. H. Chan and M. H. Pong, "Interleaved boost power factor corrector operating in discontinuous-inductor-current mode," in *Proc. Power Convers. Conf. (PCC)*, vol. 1. Nagaoka, Japan, 1997, pp. 405–410.

[12] T. Grote, H. Figge, N. Frohleke, J. Bocker, and F. Schafmeister, "Digital control strategy for multi-phase interleaved boundary mode and DCM boost PFC converters," in *Proc. IEEE Energy Convers. Congr. Expo.*, Sep. 2011, pp. 3186–3192.

[13] K. I. Hwu and Y. T. Yau, "An interleaved AC–DC converter based on current tracking," *IEEE Trans. Ind. Electron.*, vol. 56, no. 5, pp. 1456–1463, May 2009.

[14] J. Zhu and A. Pratt, "Capacitor ripple current in an interleaved PFC converter," *IEEE Trans. Power Electron.*, vol. 32, no. 10, pp. 7750–7769, Oct. 2017.

[15] H. Kim, J. Baek, M. Ryu, J. Kim, and J. Jung, "The high-efficiency isolated AC–DC converter using the three-phase interleaved *LLC* resonant converter employing the Y-connected rectifier," *IEEE Trans. Power Electron.*, vol. 29, no. 8, pp. 4017–4028, Aug. 2014.

[16] Y. Zhang, C. Li, Z. Cao, and D. Xu, "Soft-switching single-stage current-fed full-bridge isolated converter for high power AC/DC applications," in *Proc. 9th Int. Conf. Power Electron. ECCE Asia (ICPE-ECCE Asia)*, Jun. 2015, pp. 48–53.

[17] Y.-T. Chen, S. Shiu, and R. Liang, "Analysis and design of a zero-voltage-switching and zero-current-switching interleaved boost converter," *IEEE Trans. Power Electron.*, vol. 27, no. 1, pp. 161–173, Jan. 2012.

[18] M. Pahlevaninezhad, P. Das, J. Drobnik, P. K. Jain, and A. Bakhshai, "A ZVS interleaved boost AC/DC converter used in plug-in electric vehicles," *IEEE Trans. Power Electron.*, vol. 27, no. 8, pp. 3513–3529, Aug. 2012.

[19] C. M. de Oliveira Stein, J. R. Pinheiro, and H. L. Hey, "A ZCT auxiliary commutation circuit for interleaved boost converters operating in critical conduction mode," *IEEE Trans. Power Electron.*, vol. 17, no. 6, pp. 954–962, Nov. 2002.

[20] M. Rezvanyvardom, M. Mohammadi, H. Farzanehfard, and E. Adib, "Analysis, design and implementation of zero-current transition interleaved boost converter," *IET Power Electron.*, vol. 5, no. 9, pp. 1804–1812, Nov. 2012.

[21] R. Rasoulinezhad, A. Abosnina, and G. Moschopoulos, "An AC-DC interleaved ZCS-PWM boost converter with improved light-load efficiency," in *Proc. IEEE Appl. Power Electron. Conf. Expo. (APEC)*, Anaheim, CA, USA, Mar. 2019, pp. 2047–2053.

[22] K. H. M. S. Chao Yang, "High step-up interleaved converter with soft-switching using a single auxiliary switch for a fuel cell system," *IET Power Electron.*, vol. 7, no. 11, pp. 2704–2716, Nov. 2014.

[23] P. Patil and V. Agarwal, "Novel soft switched interleaved DC-DC converters for integration of renewable sources and storage into low voltage DC micro grid," in *Proc. IEEE 6th Int. Symp. Power Electron. Distrib. Gener. Syst. (PEDG)*, Aachen, Germany, Jun. 2015, pp. 1–8.

[24] P. Das and G. Moschopoulos, "A comparative study of zero-current-transition PWM converters," *IEEE Trans. Ind. Electron.*, vol. 54, no. 3, pp. 1319–1328, Jun. 2007.

[25] C. M. Wang, C. H. Lin, S. Y. Hsu, C. M. Lu, and J. C. Li, "Analysis, design and performance of a zero-current-switching pulse-width-modulation interleaved boost DC/DC converter," *IET Power Electron.*, vol. 7, no. 9, pp. 2437–2445, Sep. 2014.

[26] W. Li, W. Li, X. Xiang, Y. Hu, and X. He, "High step-up interleaved converter with built-in transformer voltage multiplier cells for sustainable energy applications," *IEEE Trans. Power Electron.*, vol. 29, no. 6, pp. 2829–2836, Jun. 2014.

[27] A. Burak, "An improved ZVT–ZCT PWM DC–DC boost converter with increased efficiency," *IEEE Trans. Power Electron.*, vol. 29, no. 4, pp. 1919–1926, Apr. 2014.

[28] H. Bahrami, E. Adib, S. Farhangi, H. Eini, and R. Golmohammadi, "ZCS-PWM interleaved boost converter using resonance-clamp auxiliary circuit," *IET Power Electron.*, vol. 10, no. 3, pp. 405–412, 2017.

[29] M. Rezvanyvardom, A. Mirzaei, and S. Rahimi, "New interleaved fully soft switched pulse width modulation boost converter with one auxiliary switch," *IET Power Electron.*, vol. 12, no. 5, pp. 1053–1060, May 2019.

[30] S.-H. Park, G.-R. Cha, Y.-C. Jung, and C.-Y. Won, "Design and application for PV generation system using a soft-switching boost converter with SARC," *IEEE Trans. Ind. Electron.*, vol. 57, no. 2, pp. 515–522, Feb. 2010.
[31] M. Rezvanyvardom, E. Adib, and H. Farzanehfard, "New interleaved zero-current switching pulse-width modulation boost converter with one auxiliary switch," *IET Power Electron.*, vol. 4, no. 9, pp. 979–983, 2011.
[32] T. Mishima, Y. Takeuchi, and M. Nakaoka, "Analysis, design, and performance evaluations of an edge-resonant switched capacitor cell-assisted soft-switching PWM boost DC–DC converter and its interleaved topology," *IEEE Trans. Power Electron.*, vol. 28, no. 7, pp. 3363–3378, Jul. 2013.
[33] I. Ando, K. Abe, M. Ochiai, and K. Ohishi, "Soft-switching-interleaved power factor correction converter with lossless snubber," in *Proc. 39th Annu. Conf. IEEE Ind. Electron. Soc. (IECON)*, Vienna, Austria, Nov. 2013, pp. 7216–7221.
[34] G. Yao, A. Chen, and X. He, "Soft switching circuit for interleaved boost converters," *IEEE Trans. Power Electron.*, vol. 22, no. 1, pp. 80–86, Jan. 2007.
[35] M. Li, B. Zhang, D. Qiu, and G. Zhang, "Sneak circuit phenomena in a DCM boost converter considering parasitic parameters," *IEEE Trans. Power Electron.*, vol. 32, no. 5, pp. 3946–3958, May 2017.
[36] H.-S. Choi and B. Hyung Cho, "Novel zero-current-switching (ZCS) PWM switch cell minimizing additional conduction loss," *IEEE Trans. Ind. Electron.*, vol. 49, no. 1, pp. 165–172, Feb. 2002.
[37] S. Sathyan, H. M. Suryawanshi, B. Singh, C. Chakraborty, V. Verma, and M. S. Ballal, "ZVS–ZCS high voltage gain integrated boost converter for DC microgrid," *IEEE Trans. Ind. Electron.*, vol. 63, no. 11, pp. 6898–6908, Nov. 2016.
[38] S. Sathyan, H. M. Suryawanshi, M. S. Ballal, and A. B. Shitole, "Soft-switching DC–DC converter for distributed energy sources with high step-up voltage capability," *IEEE Trans. Ind. Electron.*, vol. 62, no. 11, pp. 7039–7050, Nov. 2015.
[39] G. Moschopoulos, P. K. Jain, Y.-F. Liu, and G. Joos, "A zero-voltage-switched PWM boost converter with an energy feedforward auxiliary circuit," *IEEE Trans. Power Electron.*, vol. 14, no. 4, pp. 653–662, Jul. 1999.
[40] R. Rasoulinezhad, A. Abosnina, and G. Moschopoulos, "A novel AC-DC interleaved ZCS-PWM boost converter," in *Proc. IEEE Appl. Power Electron. Conf. Expo. (APEC)*, Mar. 2018, pp. 716–722.
[41] [Online]. Available: http://www.igbt.cn/UserFiles/Support_IGBT/file_057.pdf

RAMTIN RASOULINEZHAD (Graduate Student Member, IEEE) received the M.Sc. degree from Iran, in 2013, and the M.Sc. degree from Western University, London, ON, Canada, in 2017, in electrical engineering with specialization in power systems and power electronics, where he is currently pursuing the Ph.D. degree in electrical engineering. He has worked as an Electrical Design Engineer in various industrial projects. He currently works as the Director of Hybrid Solutions for an energy innovation company (AVL), Hamilton, ON, Canada. His research interests include integrating of hybrid distributed energy resources, such as gas generators, energy storage systems, and renewable energies by considering power systems and power electronics features. He is a member of the Ontario Society of Professional Engineers (OSPE) and a Subject Matter Expert (SME) for OSPE's Energy Task Force.

ADEL ALI ABOSNINA (Student Member, IEEE) received the B.Sc. degree and the M.Sc. degree in electrical and electronic engineering from Benghazi University, Benghazi, Libya, in 1998 and 2008, respectively, and the Ph.D. degree in electrical engineering from Western University, London, ON, Canada, in 2020.

From 1999 to 2013, he was an Instructor, a Lecturer Assistant, and a Lecturer with the College of Electrical and Electronics Technology, Benghazi. From 2009 to 2012, he has worked as a part-time Lecturer with Benghazi University. He is currently a Postdoctoral Associate with Western University. His research interests include power electronic converters for renewable energy and utility applications, renewable energy systems, and microcontroller applications.

JAVAD KHODABAKHSH (Member, IEEE) received the M.Sc. degree in electrical engineering from the University of Tehran, Tehran, Iran, in 2006, and the Ph.D. degree in electrical engineering from Western University, London, ON, Canada, in 2019. From 2007 to 2015, he was a tenured Lecturer with Azad University, Tehran, where he is currently working as an Electrical Design Engineer in various industrial projects (oil and gas and mine and metal). He is also a Lecturer with Western University. His research interests include power electronic converters for utility applications, transactive energy, microgrid operation, and renewable energy systems. He is a member of the Ontario Society of Professional Engineers (OSPE).

GERRY MOSCHOPOULOS (Senior Member, IEEE) received the B.Eng., M.A.Sc., and Ph.D. degrees in electrical engineering from Concordia University, Montreal, QC, Canada, in 1989, 1992, and 1997, respectively. From 1996 to 1998, he was a Design Engineer with the Advanced Power Systems Division, Nortel Networks, Lachine, QC, Canada. From 1998 to 2000, he was a Postdoctoral Fellow with Concordia University, where he was involved in research in the area of power electronics for telecommunications applications. He joined the Department of Electrical and Computer Engineering, Western University, London, ON, Canada, in 2000, where he is currently a Professor. He has authored or coauthored more than 200 technical articles and one book. He was the Co-Technical Chair of the IEEE International Communications Energy Conference (INTELEC), in 2014, the Co-Technical Chair of the IEEE Canadian Conference on Electrical and Computer Engineering (CCECE), in 2012 and 2014, and the Technical Chair of the IEEE Electrical Power and Energy Conference (EPEC), in 2015. He is an Associate Editor of the IEEE TRANSACTIONS ON POWER ELECTRONICS and the IEEE JOURNAL OF EMERGING AND SELECTED TOPICS IN POWER ELECTRONICS. He is a Registered Professional Engineer in Ontario.